A control volume technique based on integrated RBFNs for the convection-diffusion equation

N. Mai-Duy* and T. Tran-Cong

Faculty of Engineering and Surveying,

The University of Southern Queensland, Toowoomba, QLD 4350, Australia

Submitted to *Numerical Methods for Partial Differential Equations*,

5-Sep-2008; revised, 27-Nov-2008

*Corresponding author: Telephone +61 7 4631 1324, Fax +61 7 4631 2526, E-mail maiduy@usq.edu.au

Abstract This paper reports a new high-order control-volume discretisation for the convection-diffusion equation in one and two dimensions. Diffusive fluxes at the faces of a control volume and other terms embracing the unknown field variable are all approximated using one-dimensional integrated radial-basis-function networks; line integrals involving these fluxes and other integrals are evaluated using a high-order numerical integration scheme. The accuracy of the proposed technique is investigated numerically through the solution of several linear and nonlinear test problems, including a benchmark thermally-driven cavity flow. High-order convergence solutions are obtained.

Key words: Control volumes; integrated radial basis function networks; convection-diffusion equations

1 INTRODUCTION

Over the past 25 years, control-volume methods (CVMs)/finite-volume methods (FVMs) have been very popular in the simulation of heat transfer and fluid flow problems (e.g. [1,2]). The reasons for the popularity of CVMs are (i) their conservative nature, (ii) their ability to handle domains with complex geometry, and (iii) their ability to generate economical solutions. The CV formulation is based on the actual satisfaction of the physical laws (i.e. the conservations of mass, momentum and energy) rather than on the satisfaction of approximate discrete expressions controlled by means of mesh size. Like finite-element methods (FEMs), CVMs also rely on the subdivision of the problem domain into a set of subdomains called finite-volumes/control-volumes. Unlike FEMs, the governing differential equation here is directly integrated over these volumes (i.e. the weighting function is chosen to be unity in a control volume), where calculations required embrace the approximation of diffusive fluxes at the surfaces of the control volume and the evaluation of surface integrals involving these fluxes. These approximations have a strong influence on the overall accuracy of a CV solution. Here, we refer to CVMs described in the

book of Patankar [1] as a standard/classical CV scheme, in which numerical integration is performed via the midpoint rule and gradients are approximated using linear shape functions. In recent years, considerable effort has been put into the development of new techniques that enhance the flux prediction (e.g. [3-8]).

Radial-basis-function networks (RBFNs) are considered as a powerful numerical tool for the approximation of scattered data. The RBFN approximations are constructed using a set of distinct points that can be randomly distributed rather than a set of elements that are defined by a fixed typology. RBFNs have the universal approximation property (i.e. they can represent any continuous function to a prescribed level of accuracy). A number of RBFs such as the multiquadric and Gaussian basis functions exhibit an exponential rate of convergence. As a result, RBFNs have found applications in many different fields of industrial and academic interests. In computational mechanics, meshless RBFN collocation methods, originally derived by Kansa [9], have received a great deal of attention from both engineering and scientific research communities (e.g. [10-14] and references therein). Very accurate solutions can be achieved using relatively small numbers of interpolating points. However, conventional RBFN collocation methods still suffer from the following problems: (i) mathematical theories for determining optimal values for the network parameters such as the RBF width are still lacking and (ii) the interpolation RBF matrices are generally ill-conditioned (i.e. the matrix condition number grows very fast with increasing number of RBFs used). The latter limits the use of RBFNs to discretised systems with only a few hundreds of points. Local RBF approximation methods (e.g. [12]) and multi-domain RBF methods (e.g. [11]) provide a good way to overcome this problem. Recently, a numerical scheme, based on one-dimensional integrated RBFNs (1D-IRBFNs), point collocation and Cartesian grids, for solving differential problems in regular and irregular domains was reported in [15,16]. The use of integration to construct the RBF approximations is expected to overcome the problem of reduced convergence rate caused by differentiation, while the employment of 1D interpolation schemes in solv-

ing 2D problems leads to a significant improvement in the matrix condition number and computational effort. Numerical results showed that this RBF technique allows a much larger number of nodes to be employed.

Apart from the above implementations, RBFNs are also introduced into conventional discretisation techniques such as FEMs and CVMs to represent the field variables. There has been an increased level of interest in this type of application. For example, in the context of CVMs, Moroney and Turner [6,7] and Orsini, Power and Morvan [8] replaced linear/quadratic shape functions with RBFs to improve the accuracy of a flux approximation. In addition, to make CV-RBF schemes more accurate, surface integrals were evaluated using a high-order numerical integration scheme (i.e. Gaussian quadrature) [6,7], or the RBF interpolation schemes were also constructed to satisfy the governing equation at some auxiliary points on a cell stencil [8]. Numerical experiments showed that CV-RBF methods can yield accurate solutions on a much coarser mesh than standard CV methods. They thus have the ability to reduce the computational effort required for a given degree of accuracy. In [7], a comparison of CPU time between CV-RBF and CV-FE methods was made, indicating the former is more efficient than the latter for a given accuracy.

In this study, we present a CV technique incorporating 1D-IRBFNs for the diffusion-convection equation in one and two dimensions. Like CV-RBF techniques [6,7], line integrals embracing gradients are evaluated here using Gaussian quadrature. In the case of Neumann boundary conditions, the present IRBFN interpolation scheme is constructed to satisfy not only the field variable at every grid node, but also the boundary derivative values. Numerical results show that (i) the matrix condition number is as low as that yielded through standard CVMs and (ii) high-order convergence solutions are achieved. The proposed technique will be referred to as the 1D-IRBFN CV method.

The remainder of the paper is organised as follows. A short review of the control-volume

formulation is given in Section 2. In Section 3, we briefly present the 1D-IRBFN interpolation scheme. The proposed CVM is described in Section 4 through the solution of linear and nonlinear test problems including a benchmark natural convection in a square cavity. Section 5 concludes the paper.

2 CONTROL-VOLUME FORMULATION

A control-volume approach is well documented in the literature. Its fundamentals can be found in the book of Patankar [1]. For the sake of completeness, a brief review of the formulation is given below.

Consider the convection-diffusion equation defined as

$$\frac{\partial}{\partial t}(\rho\phi) + \nabla.\,(\rho\widehat{u}\phi) - \nabla.\,(\kappa\nabla\phi) + R = 0, \quad \widehat{x} \in \Omega, \tag{1}$$

with a set of the initial and boundary conditions. In (1), ϕ is the field variable, t the time, ρ the density, $\widehat{u}$ the convection velocity vector, κ the diffusion coefficient, R the source term, $\widehat{x}$ the position vector and Ω the domain of interest.

The above equation presents the conservation principle for ϕ over an infinitesimal control volume (i.e. there is a balance between the rate of change of ϕ, the convective flux rate, the diffusion flux rate, and the generation rate).

The control-volume approach subdivides the problem domain into a set of control volumes in such a way that there is one control volume surrounding each nodal point. By directly integrating (1) over a control volume V, the following equation is obtained

$$\int_V \left(\frac{\partial}{\partial t}(\rho\phi) + \nabla.\,(\rho\widehat{u}\phi) - \nabla.\,(\kappa\nabla\phi) + R \right) dV = 0 \tag{2}$$

which possesses the conservative property for ϕ for a finite control volume.

Applying the Gauss divergence theorem to (2) results in

$$\frac{\partial}{\partial t}\int_V (\rho\phi)dV + \int_S (\rho\widehat{u}\phi)\,.\widehat{n}dS - \int_S (\kappa\nabla\phi)\,.\widehat{n}dS + \int_V RdV = 0, \tag{3}$$

where S is the boundaries of V, $\widehat{n}$ is the unit outward vector normal to S, and dS is a differential element of S. The governing differential equation (1) is thus transformed into a CV form (2)/(3). It is noted that no approximation is made at this stage. Attractive features of the CV approach include (i) physical quantities such as mass, momentum, and energy are conserved over every control volume and therefore over the whole computational domain, regardless of the number of nodal points used, (ii) a Neumann boundary condition can be incorporated straightforwardly into the CV equation set because these equations contain first derivative terms explicitly, and (iii) one only needs to use discrete expressions representing the field variable and its first derivatives for the discretisation of second-order differential equations.

From a mathematical point of view, equation (2) is equivalent to the weighted-residual statement with the chosen weighting functions being unity in a control volume and zero outside a control volume (the subdomain collocation method). However, the control-volume approach is more physically meaningful than the weighted-residual approach.

3 ONE-DIMENSIONAL INTEGRATED RBFNS

This study is concerned with the numerical solution of the convection-diffusion equation (second-order PDE). The basic idea of the integral RBF scheme [17,18] is to decompose the highest-order derivatives of ϕ in a given differential equation (i.e. the second-order ones here) into RBFs. Consider a univariate function $\phi(x)$. The present 1D-IRBFN

scheme starts with

$$\frac{d^2\phi(x)}{dx^2} = \sum_{i=1}^{N_x} w_i I_i^{(2)}(x), \tag{4}$$

where $\{w_i\}_{i=1}^{N_x}$ is the set of network weights and $\left\{I_i^{(2)}(x)\right\}_{i=1}^{N_x}$ is the set of RBFs. Expressions for the first-order derivative and function itself are then obtained through integration

$$\frac{d\phi(x)}{dx} = \sum_{i=1}^{N_x} w_i I_i^{(1)}(x) + c_1, \tag{5}$$

$$\phi(x) = \sum_{i=1}^{N_x} w_i I_i^{(0)}(x) + c_1 x + c_2, \tag{6}$$

where $I_i^{(1)}(x) = \int I_i^{(2)}(x)dx$, $I_i^{(0)}(x) = \int I_i^{(1)}(x)dx$, and (c_1, c_2) are the constants of integration. It is noted that the superscript $(.)$ is used to indicate the derivative order of ϕ which the basis functions $I_i(x)$ are associated with.

Evaluation of (4)-(6) at a set of collocation points $\{x_i\}_{i=1}^{N_x}$ leads to

$$\widehat{\frac{d^2\phi}{dx^2}} = \widehat{\mathcal{I}}^{(2)}\widehat{\alpha}, \tag{7}$$

$$\widehat{\frac{d\phi}{dx}} = \widehat{\mathcal{I}}^{(1)}\widehat{\alpha}, \tag{8}$$

$$\widehat{\phi} = \widehat{\mathcal{I}}^{(0)}\widehat{\alpha}, \tag{9}$$

where

$$\widehat{\mathcal{I}}^{(2)} = \begin{bmatrix} I_1^{(2)}(x_1), & I_2^{(2)}(x_1), & \cdots, & I_{N_x}^{(2)}(x_1), & 0, & 0 \\ I_1^{(2)}(x_2), & I_2^{(2)}(x_2), & \cdots, & I_{N_x}^{(2)}(x_2), & 0, & 0 \\ \vdots & \vdots & \ddots & \vdots & \vdots & \vdots \\ I_1^{(2)}(x_{N_x}), & I_2^{(2)}(x_{N_x}), & \cdots, & I_{N_x}^{(2)}(x_{N_x}), & 0, & 0 \end{bmatrix},$$

$$\widehat{\mathcal{I}}^{(1)} = \begin{bmatrix} I_1^{(1)}(x_1), & I_2^{(1)}(x_1), & \cdots, & I_{N_x}^{(1)}(x_1), & 1, & 0 \\ I_1^{(1)}(x_2), & I_2^{(1)}(x_2), & \cdots, & I_{N_x}^{(1)}(x_2), & 1, & 0 \\ \vdots & \vdots & \ddots & \vdots & \vdots & \vdots \\ I_1^{(1)}(x_{N_x}), & I_2^{(1)}(x_{N_x}), & \cdots, & I_{N_x}^{(1)}(x_{N_x}), & 1, & 0 \end{bmatrix},$$

$$\widehat{\mathcal{I}}^{(0)} = \begin{bmatrix} I_1^{(0)}(x_1), & I_2^{(0)}(x_1), & \cdots, & I_{N_x}^{(0)}(x_1), & x_1, & 1 \\ I_1^{(0)}(x_2), & I_2^{(0)}(x_2), & \cdots, & I_{N_x}^{(0)}(x_2), & x_2, & 1 \\ \vdots & \vdots & \ddots & \vdots & \vdots & \vdots \\ I_1^{(0)}(x_{N_x}), & I_2^{(0)}(x_{N_x}), & \cdots, & I_{N_x}^{(0)}(x_{N_x}), & x_{N_x}, & 1 \end{bmatrix};$$

$$\widehat{\alpha} = (w_1, w_2, \cdots, w_{N_x}, c_1, c_2)^T;$$

and

$$\widehat{\frac{d^k\phi}{dx^k}} = \left(\frac{d^k\phi_1}{dx^k}, \frac{d^k\phi_2}{dx^k}, \cdots, \frac{d^k\phi_{N_x}}{dx^k}\right)^T, \quad k = (1, 2),$$

$$\widehat{\phi} = (\phi_1, \phi_2, \cdots, \phi_{N_x})^T,$$

in which $d^k\phi_i/dx^k = d^k\phi(x_i)/dx^k$ and $\phi_i = \phi(x_i)$ with $i = (1, 2, \cdots, N_x)$.

This use of integration to construct the RBF approximations is expected to avoid the deterioration of accuracy caused by differentiation ([5,17,18]). Numerical studies, e.g. [17,19,20], have shown that the integral collocation approach is more accurate than the differential collocation approach. Recently, theoretical studies, e.g. [21], have confirmed superior accuracy of integrated RBFNs over differentiated RBFNs.

4 THE PRESENT CV TECHNIQUE

This work is the first attempt to introduce 1D-IRBFNs into the control volume formulation to represent the field variable. Only uniform rectangular grids are considered at this stage. However, the present solution procedure can be extended to the case of non-uniform rectangular grids straightforwardly. Consider the convection-diffusion equation (1) defined on a line segment in one dimension and a rectangular domain in two dimensions. A Cartesian grid is placed on the computational domain. The approximations based on 1D-IRBFNs for the field variable and its derivatives can be constructed at the global level or locally

at the neighbouring points of a given control volume. Global approximation schemes are known to be more accurate than local schemes, but require more computational effort to construct. For problems, which do not require very dense discretisations for an accurate simulation, the use of global schemes is a preferred option. In this study, we are interested in such problems and thus implement global approximation schemes. It is noted that, for any level, 1D-IRBFNs possess some "local" characteristics in comparison with conventional RBF schemes. On a grid line, 1D-IRBFNs are employed to represent the field variable and its derivatives. Associated with grid nodes are control volumes that do not overlap each other. In this work, we implement the multiquadric (MQ) basis function whose form is

$$I_i^{(2)}(x) = \sqrt{(x - c_i)^2 + a_i^2}, \tag{10}$$

where c_i and a_i are the MQ centre and width, respectively. The present MQ width is simply chosen to be the grid size, and the set of centres $\{c_i\}_{i=1}^{N_x}$ is the set of grid points $\{x_i\}_{i=1}^{N_x}$ itself. All boundary conditions are directly imposed on the IRBFN approximations, and the governing equations are forced to be satisfied locally over control volumes by means of subregion collocation. The obtained set of algebraic equations exhibits exact integral balances, regardless of the accuracy.

We seek the solution in terms of its nodal values. It is thus necessary to carry out the conversion of the network-weight space into the physical space. A distinguishing feature of 1D-IRBFNs is that their coefficient vector $\widehat{\alpha}$ is larger owing to the presence of integration constants. As a result, one can add additional equations to the conversion system to represent "extra information" such as nodal derivative values. On a grid line,

the conversion system can be formed as follows

$$\begin{pmatrix} \widehat{\phi} \\ \widehat{f} \end{pmatrix} = \begin{bmatrix} \mathcal{I}^{(0)} \\ \mathcal{K} \end{bmatrix} \widehat{\alpha} = \mathcal{C}\widehat{\alpha}, \tag{11}$$

$$\widehat{\alpha} = \mathcal{C}^{-1} \begin{pmatrix} \widehat{\phi} \\ \widehat{f} \end{pmatrix}, \tag{12}$$

where $\widehat{f} = \mathcal{K}\widehat{\alpha}$ are additional equations whose number can be up to 2; $\widehat{\phi}$, $\widehat{\mathcal{I}}^{(0)}$ and $\widehat{\alpha}$ are defined as before; and $\mathcal{C}$ the conversion matrix. It can be seen that (11) and (12) still allow one to collocate the function ϕ at every node on the grid line including the two boundary points. We will utilise $\widehat{f}$ for the purpose of implementing a Neumann boundary condition and deriving a computational boundary condition for the vorticity in the solution of the Navier-Stokes equation. In the case of two dimensions, the corresponding basis functions are constructed as products of integrated RBFs in each direction. The present method is described in detail through the solution of several 1D and 2D problems.

4.1 1D steady-state diffusion problem

Consider a 1D problem governed by

$$\frac{d}{dx}\left(\frac{d\phi}{dx}\right) + \phi + x = 0, \quad 0 \leq x \leq 1, \tag{13}$$

with two different cases of boundary conditions: (i) Dirichlet only, and (ii) Dirichlet and Neumann conditions. The exact solution of this problem is

$$\phi_e(x) = \frac{\sin(x)}{\sin(1)} - x. \tag{14}$$

The problem domain is replaced with a set of uniform points. Each node x_i is surrounded by a control volume denoted by Ω_i (Figure 1). For $2 \leq i \leq N_x - 1$, Ω_i is defined as

$[x_{i-1/2}, x_{i+1/2}]$. For $i = 1$ and $i = N_x$, its control volume is taken to be $[x_1, x_{x_{1+1/2}}]$ and $[x_{N_x-1/2}, x_{N_x}]$, respectively (i.e. half of the interior control volume).

Integrating (13) over a control volume Ω_i, one has

$$\frac{d\phi}{dx}(x_{i+1/2}) - \frac{d\phi}{dx}(x_{i-1/2}) + \int_{x_{i-1/2}}^{x_{i+1/2}} \phi dx = -\int_{x_{i-1/2}}^{x_{i+1/2}} x dx. \tag{15}$$

To study the convergence behaviour of the present technique, a number of uniform grids with $N_x = (9, 11, 13, \cdots, 151)$ are employed.

Dirichlet boundary conditions only: For this case, $\widehat{f}$ and $\mathcal{K}$ in (11) and (12) are simply set to null. Making use of (11)-(12) and (6)-(4), the values of ϕ, $d\phi/dx$ and $d^2\phi/dx^2$ at an arbitrary point x can be computed in terms of the grid values of ϕ as

$$\phi(x) = \left[I_1^{(0)}(x), I_2^{(0)}(x), \cdots, I_{N_x}^{(0)}(x), x, 1\right] \widehat{\mathcal{C}}^{-1}\widehat{\phi}, \tag{16}$$

$$\frac{d\phi}{dx}(x) = \left[I_1^{(1)}(x), I_2^{(1)}(x), \cdots, I_{N_x}^{(1)}(x), 1, 0\right] \widehat{\mathcal{C}}^{-1}\widehat{\phi}, \tag{17}$$

$$\frac{d^2\phi}{dx^2}(x) = \left[I_1^{(2)}(x), I_2^{(2)}(x), \cdots, I_{N_x}^{(2)}(x), 0, 0\right] \widehat{\mathcal{C}}^{-1}\widehat{\phi}. \tag{18}$$

The above expressions can be rewritten as

$$\phi(x) = \sum_{i=1}^{N_x} \varphi_i(x)\phi_i, \tag{19}$$

$$\frac{d\phi}{dx}(x) = \sum_{i=1}^{N_x} \frac{d\varphi_i}{dx}(x)\phi_i, \tag{20}$$

$$\frac{d^2\phi}{dx^2}(x) = \sum_{i=1}^{N_x} \frac{d^2\varphi_i}{dx^2}(x)\phi_i, \tag{21}$$

where $\varphi_i(x)$ are the new basis functions in the physical space.

We use Gaussian quadrature to evaluate integrals in the CV equations. A system of algebraic equations is generated using (15) with $i = (2, 3, \cdots, N_x - 1)$, from which one

can find the values of ϕ at the interior grid points.

Dirichlet ($x = 0$) and Neumann ($x = 1$) conditions: For this case, the IRBFN scheme is forced to satisfy a priori the Neumann boundary condition. In (11) and (12), $\mathcal{K}$ is made up of the last row of $\mathcal{I}^{(1)}$ and $\widehat{f}$ is simply $d\phi_{N_x}/dx$.

A function ϕ and its derivatives at x can be expressed as

$$\phi(x) = \left[I_1^{(0)}(x), I_2^{(0)}(x), \cdots, I_{N_x}^{(0)}(x), x, 1\right] \widehat{\mathcal{C}}^{-1} \begin{pmatrix} \widehat{\phi} \\ \frac{d\phi_{N_x}}{dx} \end{pmatrix}, \tag{22}$$

$$\frac{d\phi}{dx}(x) = \left[I_1^{(1)}(x), I_2^{(1)}(x), \cdots, I_{N_x}^{(1)}(x), 1, 0\right] \widehat{\mathcal{C}}^{-1} \begin{pmatrix} \widehat{\phi} \\ \frac{d\phi_{N_x}}{dx} \end{pmatrix}, \tag{23}$$

$$\frac{d^2\phi}{dx^2}(x) = \left[I_1^{(2)}(x), I_2^{(2)}(x), \cdots, I_{N_x}^{(2)}(x), 0, 0\right] \widehat{\mathcal{C}}^{-1} \begin{pmatrix} \widehat{\phi} \\ \frac{d\phi_{N_x}}{dx} \end{pmatrix}, \tag{24}$$

or

$$\phi(x) = \sum_{i=1}^{N_x} \overline{\varphi}_i(x)\phi_i + \overline{\varphi}_{N_x+1}(x)\frac{d\phi_{N_x}}{dx}, \tag{25}$$

$$\frac{d\phi}{dx}(x) = \sum_{i=1}^{N_x} \frac{d\overline{\varphi}_i}{dx}(x)\phi_i + \frac{d\overline{\varphi}_{N_x+1}}{dx}(x)\frac{d\phi_{N_x}}{dx}, \tag{26}$$

$$\frac{d^2\phi}{dx^2}(x) = \sum_{i=1}^{N_x} \frac{d^2\overline{\varphi}_i}{dx^2}(x)\phi_i + \frac{d^2\overline{\varphi}_{N_x+1}}{dx^2}(x)\frac{d\phi_{N_x}}{dx}. \tag{27}$$

The notation overbar is used to indicate that extra information values are incorporated into the IRBFN approximations. An attractive feature of (22)-(24)/(25)-(27) lies in the fact that the approximate expression (22)/(25) representing ϕ satisfies the Neumann boundary condition identically. In (25), ϕ_1 and $d\phi_{N_x}/dx$ are given, and the remaining nodal values are determined by solving the equation set generated by (15) with $i = (2, 3, \cdots, N_x)$.

Results concerning the discrete relative L_2 norm of the solution ϕ, N_e, and the condition number of the system matrix, cond$A$, are presented in Figure 2. For the assessment of accuracy of the present technique, we also include results obtained by the IRBFN collocation and standard CV methods.

In terms of the matrix condition number, it can be seen that the growth in cond$A$ is at a rate of about $O(h^{-2.0})$ for the three techniques. In terms of accuracy, both IRBFN methods outperforms CVM. At $N_x = 151$, the present CV method achieves an accuracy better than that of standard CVMs by two orders of magnitude.

In the context of RBF methods, it is widely observed that collocation solutions to Dirichlet-type boundary-value problems are generally more accurate than those to problems with Neumann boundary conditions (e.g. [22]). This deterioration of accuracy also occurs here as shown in Figure 2 (Legend "collocation IRBFN"). However, via a control-volume approach, conservative IRBFN solutions to both problems have similar degrees of accuracy. It appears that subregion collocation is able to handle Neumann boundary conditions better than point collocation.

4.2 2D steady-state diffusion problem

Consider the following diffusion equation

$$\frac{\partial}{\partial x}\left(\frac{\partial \phi}{\partial x}\right) + \frac{\partial}{\partial y}\left(\frac{\partial \phi}{\partial y}\right) = 0, \tag{28}$$

on a square domain $0 \leq x, y \leq \pi$, subject to two different cases of boundary conditions that will be described shortly. The exact solution for this problem is

$$\phi_e(x, y) = \frac{1}{\sinh(\pi)} \sin(x) \sinh(y), \tag{29}$$

whose variation is shown in Figure 3.

The problem domain is discretised using a uniform Cartesian grid. For each grid point (x_i, y_j), one can construct a control volume $\Omega_{i,j}$ with its interfaces $\Gamma_{i,j}$ as shown in Figure 4. There is a full control volume for an interior node and only a half control volume for a boundary node.

The CV equation of (28) takes the form

$$\int_{\Gamma_{i,j}} \left(\frac{\partial \phi}{\partial x} dy - \frac{\partial \phi}{\partial y} dx \right) = 0, \tag{30}$$

which involves first derivatives of ϕ only. Flux integrals over line segments of $\Gamma_{i,j}$ are evaluated using Gaussian quadrature that is more straightforward to implement than analytical schemes.

Dirichlet boundary conditions only The solution ϕ is sought in the form

$$\phi(x, y) = \sum_{i=1}^{N_x} \sum_{j=1}^{N_y} \varphi_i^{(x)}(x) \varphi_j^{(y)}(y) \phi_{i,j}, \tag{31}$$

where the basis functions are products of integrated RBFs in each direction, the superscript (x)/(y) indicates that the basis function is obtained from the integration process with respect to the x/y variable, and $\phi_{i,j} = \phi(x_i, y_j)$. Algebraic equations are generated in the same manner as in the previous problem, where the values of i and j defining a grid node and its associated control volume in (30) are taken from 2 to $N_x - 1$ and 2 to $N_y - 1$, respectively.

Dirichlet ($x = 0$ and $x = \pi$) and Neumann ($y = 0$ and $y = \pi$) conditions We approximate the solution ϕ in the form

$$\phi(x,y) = \sum_{i=1}^{N_x} \varphi_i^{(x)}(x) \left(\sum_{j=1}^{N_y} \overline{\varphi}_j^{(y)}(y)\phi(x_i,y_j) + \overline{\varphi}_{N_y+1}^{(y)}(y)\frac{\partial\phi}{\partial y}(x_i,y_1) + \overline{\varphi}_{N_y+2}^{(y)}(y)\frac{\partial\phi}{\partial y}(x_i,y_{N_y}) \right). \tag{32}$$

In obtaining $\left\{\overline{\varphi}_j^{(y)}\right\}_{j=1}^{N_y+2}$, we make use of (11), where $\mathcal{K}$ consists of the first and last rows of $\widehat{\mathcal{I}}^{(1)}$, and $\widehat{f}$ is made up of the two derivative values, $\partial\phi_1/\partial y$ and $\partial\phi_{N_y}/\partial y$. The size of the discretised system here is slightly larger than that in the previous case as (30) is applied with $i = (2, 3, \cdots, N_x - 1)$ and $j = (1, 2, \cdots, N_y)$.

Computations for the two cases of boundary conditions are carried out using various grids, $3 \times 3, 5 \times 5, \cdots, 71 \times 71$. Figure 5 shows comparisons of the condition number and accuracy of the conservative IRBFN and standard CV methods. Both techniques have similar condition numbers, but the former yields much faster convergence than the latter. At $N = 5041$ ($N = N_x N_y$), the present method produces a solution several orders of magnitude more accurate than that by standard CVMs. It can be seen that standard CVMs need a very fine grid in order to achieve accuracy that is comparable to the IRBFN-CV method. Like in the case of 1D problems, conservative IRBFN solutions to Dirichlet and Dirichlet-Neumann problems have similar degrees of accuracy.

4.3 1D unsteady diffusion problem

Consider the transient temperature distribution in a one dimensional slab governed by

$$\frac{\partial\phi}{\partial t} = \frac{\partial}{\partial x}\left(\frac{\partial\phi}{\partial x}\right), \tag{33}$$

where $0 \leq x \leq 1$ and $0 \leq t \leq t_f$, with the initial solution

$$\phi(x,0) = \left\{ \begin{array}{rl} 2x & \text{if} \quad 0 \leq x \leq 0.5, \\ 2(1-x) & \text{if} \quad 0.5 \leq x \leq 1. \end{array} \right), \tag{34}$$

and Dirichlet boundary conditions

$$\phi(0,t) = 0, \tag{35}$$

$$\phi(1,t) = 0. \tag{36}$$

The analytical solution is given by [23]

$$\phi_e(x,t) = \frac{8}{\pi^2} \sum_{k=1}^{\infty} \frac{1}{k^2} \sin \frac{k\pi}{2} \sin k\pi x \exp(-(k\pi)^2 t). \tag{37}$$

Haberland and Lahrmann [24] used a centred finite-difference (FD) scheme to solve this problem, where comparative investigations on recurrence formulae such as the Euler, Crank-Nicolson (CN), Pure Implicit (PI) and Weighted time step (WI) schemes are conducted. Their results with $t_f = 0.25$, $\Delta t = 0.025$ and $\Delta x = 0.05$ are included here for comparison purposes. It is noted that FD and CV formulations lead to the same discrete expressions in many cases when orthogonal coordinates are employed. For example, to this problem, the centred FD scheme is identical to the standard CV equation.

The spatial ($0 \leq x \leq 1$) and time ($0 \leq t \leq t_f$) domains are discretised here using N_x and N_t uniform points, respectively. We seek an approximate solution in the form

$$\phi(x,t) = \sum_{j=1}^{N_t} \sum_{i=1}^{N_x} \varphi^{(x)}(x_i) \varphi^{(t)}(t_j) \phi(x_i, t_j), \tag{38}$$

where the centres t_js are referred to as time levels and the grid size $\Delta t = t_j - t_{j-1}$ is considered as time step.

The discretisation equation is derived by integrating (33) over the control volume from $x_{i-1/2}$ to $x_{i+1/2}$ and the time interval from 0 to t_j

$$\int_{x_{i-1/2}}^{x_{i+1/2}} \int_0^{t_j} \frac{\partial \phi}{\partial t} dt dx = \int_0^{t_j} \int_{x_{i-1/2}}^{x_{i+1/2}} \frac{\partial^2 \phi}{\partial x^2} dx dt. \tag{39}$$

The above equation reduces to

$$\int_{x_{i-1/2}}^{x_{i+1/2}} (\phi(x, t_j) - \phi(x, 0))\, dx = \int_0^{t_j} \left(\frac{\partial \phi}{\partial x}(x_{i+1/2}, t) - \frac{\partial \phi}{\partial x}(x_{i-1/2}, t) \right) dt. \tag{40}$$

Making use of (38), both LHS and RHS of (40) can be rewritten in terms of nodal variable values $\phi_{i,j} = \phi(x_i, t_j)$. Since the function ϕ is given at $x = 0$ and $x = 1$ (the boundary conditions) and $t = 0$ (the initial solution), the unknown vector consists of the nodal values of ϕ at (x_i, t_j) with $i = (2, 3, \cdots, N_x - 1)$ and $j = (2, 3, \cdots, N_t)$. To determine this unknown vector, one needs to generate a set of $(N_x - 2)(N_t - 1)$ algebraic equations. This can be achieved by using (40) with $i = (2, 3, \cdots, N_x - 1)$ and $j = (2, 3, \cdots, N_t)$.

Unlike standard CVMs, the present technique employs global high-order approximations, and information from all previous time levels are directly used to calculate the temporal integral at the present time level. Solutions over the temporal domain is obtained at once rather than by the usual way of step by step.

Using the same time step ($\Delta t = 0.025$) and a coarser spatial discretisation ($\Delta x = 0.25$), results by conservative IRBFNs are much more accurate than those by FDMs (Table 1). The present maximum error is only 2.12%, while they are up to 14.47%, 30.76% and 27.58% for FDM-CN, FDM-PI and FDM-WI, respectively. Furthermore, it appears that the present errors do not accumulate in time. We also study the behaviour of mesh convergence of the present technique. When refining a mesh, much greater accuracy is achieved. The maximum error reduces to 0.81% for ($N_x = 7, N_t = 21$) and 0.10% for ($N_x = 9, N_t = 41$). It can thus be seen that the IRBFN-CV method is able to produce a very high degree of accuracy using a relatively coarse grid.

4.4 Thermally-driven cavity flow problem

The 1D-IRBFN CV technique is applied to simulate natural convection in a square slot. The flow is caused by density variations. However, under the Boussinesq approximation, one still has the continuity equation for a constant density fluid and the viscous stress can be evaluated as in the Navier-Stokes equation.

Consider a unit square cavity ($0 \leq x, y \leq 1$) that is stationary. The two side walls are heated with $T = 0.5$ at $x = 0$ and $T = -0.5$ at $x = 1$, while the top and bottom walls are insulated ($\partial T/\partial y = 0$ at $y = 0$ and $y = 1$).

The dimensionless governing equations for this type of flow can be written in terms of stream function ψ, vorticity ω and temperature T as

$$\frac{\partial T}{\partial t} + \sqrt{R_a P_r}\left(\frac{\partial (uT)}{\partial x} + \frac{\partial (vT)}{\partial y}\right) = \frac{\partial^2 T}{\partial x^2} + \frac{\partial^2 T}{\partial y^2}, \tag{41}$$

$$-\omega = \frac{\partial^2 \psi}{\partial x^2} + \frac{\partial^2 \psi}{\partial y^2}, \tag{42}$$

$$\frac{\partial \omega}{\partial t} + \sqrt{\frac{R_a}{P_r}}\left(\frac{\partial (u\omega)}{\partial x} + \frac{\partial (v\omega)}{\partial y} - \frac{\partial T}{\partial x}\right) = \frac{\partial^2 \omega}{\partial x^2} + \frac{\partial^2 \omega}{\partial y^2}, \tag{43}$$

where u and v are the two components of the velocity vector ($u = \partial\psi/\partial y$ and $v = -\partial\psi/\partial x$), R_a is the Rayleigh number and P_r the Prandtl number.

Integrating (41)-(43) over a control volume $\Omega_{i,j}$ leads to the following equation set

$$\frac{\partial}{\partial t}\int_{\Omega_{i,j}} T d\,\Omega_{i,j} + \int_{\Omega_{i,j}} \sqrt{R_a P_r}\left(\frac{\partial(uT)}{\partial x} + \frac{\partial(vT)}{\partial y}\right) d\,\Omega_{i,j} = \int_{\Omega_{i,j}} \left(\frac{\partial^2 T}{\partial x^2} + \frac{\partial^2 T}{\partial y^2}\right) d\,\Omega_{i,j}, \tag{44}$$

$$-\int_{\Omega_{i,j}} \omega d\,\Omega_{i,j} = \int_{\Omega_{i,j}} \left(\frac{\partial^2 \psi}{\partial x^2} + \frac{\partial^2 \psi}{\partial y^2}\right) d\,\Omega_{i,j}, \tag{45}$$

$$\frac{\partial}{\partial t}\int_{\Omega_{i,j}} \omega d\,\Omega_{i,j} + \int_{\Omega_{i,j}} \sqrt{\frac{R_a}{P_r}}\left(\frac{\partial(u\omega)}{\partial x} + \frac{\partial(v\omega)}{\partial y} - \frac{\partial T}{\partial x}\right) d\,\Omega_{i,j} = \int_{\Omega_{i,j}} \left(\frac{\partial^2 \omega}{\partial x^2} + \frac{\partial^2 \omega}{\partial y^2}\right) d\,\Omega_{i,j}. \tag{46}$$

A high-order scheme to approximate the time derivative term, which is described in Section 4.3, can be applied here. However, for the present problem, we are only interested in the steady state of the flow. Time derivative terms are used for the purpose of handling a non-linear system of algebraic equations. As a result, low-order approximation schemes are chosen and implemented for efficient purposes. In the evaluation of the first terms of (44) and (46), we assume that T and ω are constant over the control volume $\Omega_{i,j}$ and linear over the time interval (t_{k-1}, t_k). The time derivative terms reduce to

$$\int_{\Omega_{i,j}} \frac{\partial T}{\partial t} d\,\Omega_{i,j} = \frac{\int_{\Omega_{i,j}} T_{i,j,k} d\,\Omega_{i,j} - \int_{\Omega_{i,j}} T_{i,j,k-1} d\,\Omega_{i,j}}{\Delta t} = \frac{A_{i,j}}{\Delta t}\left(T_{i,j,k} - T_{i,j,k-1}\right) \tag{47}$$

$$\int_{\Omega_{i,j}} \frac{\partial \omega}{\partial t} d\,\Omega_{i,j} = \frac{\int_{\Omega_{i,j}} \omega_{i,j,k} d\,\Omega_{i,j} - \int_{\Omega_{i,j}} \omega_{i,j,k-1} d\,\Omega_{i,j}}{\Delta t} = \frac{A_{i,j}}{\Delta t}\left(\omega_{i,j,k} - \omega_{i,j,k-1}\right), \tag{48}$$

where $A_{i,j}$ is the area of the control volume $\Omega_{i,j}$.

We seek the solutions for ψ and ω in the following forms

$$\psi(x,y) = \sum_{i=1}^{N_x}\sum_{j=1}^{N_y} \varphi_i^{(x)}(x)\varphi_j^{(y)}(y)\psi_{i,j}, \tag{49}$$

$$\omega(x,y) = \sum_{i=1}^{N_x}\sum_{j=1}^{N_y} \varphi_i^{(x)}(x)\varphi_j^{(y)}(y)\omega_{i,j}, \tag{50}$$

and the solution for T as

$$T(x,y)=\sum_{i=1}^{N_x}\varphi_i^{(x)}(x)\left(\sum_{j=1}^{N_y}\overline{\varphi}_j^{(y)}(y)T_{i,j}+\overline{\varphi}_{n_{y+1}}^{(y)}(y)\frac{\partial T_{i,1}}{\partial y}+\overline{\varphi}_{n_{y+2}}^{(y)}(y)\frac{\partial T_{i,N_y}}{\partial y}\right). \tag{51}$$

Since (51) contains information about derivative boundary conditions, it is straightforward to implement the boundary conditions for T in the solution of (44). The associated unknown vector consists of the values of T at the interior nodes and at the boundary nodes on the top and bottom walls. As a result, we use (44) with $2\leq i\leq N_x-1$ and $1\leq j\leq N_y$ to generate a set of algebraic equations for T.

The cavity is stationary, leading to $\psi=0$ and $\partial\psi/\partial n=0$ on all the boundaries. We take $\psi=0$ as boundary conditions for ψ in solving (45) and use $\partial\psi/\partial n=0$ to derive a computational boundary condition for ω in solving (46). On the walls, the vorticity is computed as $\omega=-\partial^2\psi/\partial n^2$ and one has to incorporate $\partial\psi/\partial n=0$ into $\partial^2\psi/\partial n^2$. Consider a lth horizontal grid line, the values of ω at the two extreme points can be computed as

$$\omega_{l,1}=\sum_{i=1}^{N_x}\frac{d^2\overline{\varphi}_i^{(x)}}{dx^2}(x_1)\psi_{l,i}+\frac{d^2\overline{\varphi}_{N_x+1}^{(x)}}{dx^2}(x_1)\frac{\partial\psi_{l,1}}{\partial x}+\frac{d^2\overline{\varphi}_{N_x+2}^{(x)}}{dx^2}(x_1)\frac{\partial\psi_{l,N_x}}{\partial x}, \tag{52}$$

$$\omega_{l,N_x}=\sum_{i=1}^{N_x}\frac{d^2\overline{\varphi}_i^{(x)}}{dx^2}(x_{N_x})\psi_{l,i}+\frac{d^2\overline{\varphi}_{N_x+1}^{(x)}}{dx^2}(x_{N_x})\frac{\partial\psi_{l,1}}{\partial x}+\frac{d^2\overline{\varphi}_{N_x+2}^{(x)}}{dx^2}(x_{N_x})\frac{\partial\psi_{l,N_x}}{\partial x}. \tag{53}$$

Because of $\partial\psi/\partial n=0$, (52) and (53) become

$$\omega_{l,1}=\sum_{i=1}^{N_x}\frac{d^2\overline{\varphi}_i^{(x)}}{dx^2}(x_1)\psi_{l,i}, \tag{54}$$

$$\omega_{l,N_x}=\sum_{i=1}^{N_x}\frac{d^2\overline{\varphi}_i^{(x)}}{dx^2}(x_{N_x})\psi_{l,i}. \tag{55}$$

These treatments are limited to the case of flat boundaries. For curved boundaries, the present approach is applicable if, for example, a Cartesian grid is generated in a way

that the boundary points are also regular grid nodes. One is then able to apply the proposed boundary approach in both coordinate directions at a boundary point to derive a computational boundary for the vorticity. The reader is referred to [25] for how to generate such a Cartesian grid.

Equations for ψ and ω are thus subject to Dirichlet boundary conditions and hence (45) and (46) are employed with $2 \leq i \leq N_x - 1$ and $2 \leq j \leq N_y - 1$.

A time marching scheme is adopted to get the structure of a steady flow. The steady-state solution is considered as the asymptotic time limit of the time-dependent equations. At each time level, equations for T, ψ and ω are treated as separate systems. The diffusive and convective terms are treated implicitly and explicitly, respectively. It can be seen that the system matrices, which are generated from the RHS terms of (44)-(46), remain unchanged during the iteration process. The solution procedure involves the following steps

1. Guess the distributions of the temperature, stream function and vorticity
2. Solve (44) for T subject to Dirichlet and Neumann boundary conditions
3. Solve (45) for ψ subject to Dirichlet conditions
4. Compute the boundary values of ω using (54) and (55)
5. Solve (46) for ω subject to Dirichlet conditions
6. Check to see whether the solution has reached a steady state
7. If it is not satisfied, advance time step and repeat from step 2. Otherwise, stop the computation and output the results.

A wide range of R_a, $(10^3, 10^4, \cdots, 10^7)$, is considered. We take the computed solution at the lower and nearest value of R_a as the initial solution. For $R_a = 10^3$, we simply start with the fluid at rest. It is known that the strengths of boundary layers are significantly increased with increasing R_a. They become very stiff when $R_a \geq 10^6$. Benchmark solutions were reported in [26] for $10^3 \leq R_a \leq 10^6$ using a finite difference technique and in

[27] for $R_a \geq 10^6$ using a pseudospectral technique. It is noted that there are relatively few reports on the numerical simulation of the flow for $R_a > 10^6$.

Some important measures associated with this type of flow are

- Maximum horizontal velocity u_{max} on the vertical mid-plane and its location;
- Maximum vertical velocity v_{max} on the horizontal mid-plane and its location;
- The average Nusselt number throughout the cavity, which is defined as

$$\overline{N_u} = \int_0^1 N_u(x)dx, \tag{56}$$

$$N_u(x) = \int_0^1 (uT - \frac{\partial T}{\partial x})dy. \tag{57}$$

Convergence behaviour: Simulations are carried out using 6 uniform grids, $(21 \times 21, 31 \times 31, \cdots, 71 \times 71)$. Time steps are used in the range of 5×10^{-6} to 1×10^{-3}. Smaller time steps are needed for higher Ra number and denser grids. No under-relaxation is employed here. For brevity, we only present the results for flow of the highest value of R_a, where one meets the most difficult case of convergence. Grid convergence is studied both qualitatively and quantitatively. For the former, Figures 6, 8 and 7 display the stream function, vorticity and temperature fields with the three grids, 31×31, 51×51 and 71×71. It can be seen that all fields especially for ψ and T converge very fast with mesh refinement. In the case of ω whose variation is much more complex, a denser grid (e.g. 51×51) is required to provide a feasible solution. For the latter, Table 2 shows a fast rate of convergence achieved for v_{max}, u_{max} and $\overline{N_u}$ using the last four grids.

Solution accuracy: The results at 71×71 for various R_a values are given in Table 3. It can be seen they are in very good agreement with the benchmark solutions. For $R_a = 10^6$, the percentage errors are computed relative to the benchmark spectral results.

It can be seen that the present results are closer to the benchmark spectral solutions than the FD ones. It is noted that local RBF collocation techniques are also able to produce accurate simulations for high values of the Rayleigh number as shown in recent work of Kosec and Sarler [28].

5 CONCLUDING REMARKS

In this paper, 1D-IRBFNs are introduced into the CV formulation to represent the field variable and its derivatives for the convection-diffusion equation. This use of RBFs leads to a significant improvement in accuracy over the use of low-order shape functions such as linear polynomials. The IRBFN approximations are constructed "locally", i.e. the discrete expressions at a point in a 2D grid involve only nodal points on the grid lines passing through that point instead of the whole set of grid points. Derivative boundary values are incorporated into the RBF approximations in an exact manner, hence Neumann boundary conditions are satisfied identically in the CV form. Numerical results show that (i) the matrix condition number grows as low as that produced by standard CVMs, making this present formulation attractive in the context of RBF techniques, and (ii) high-order convergence solutions are obtained, including those for natural convection in a square slot. This study further demonstrates RBFs as a powerful new interpolation tool in the discretisation of PDEs.

Acknowledgement

This work is supported by the Australian Research Council. We would like to thank the referees for their helpful comments.

References

1. S.V. Patankar, *Numerical Heat Transfer and Fluid Flow*, McGraw-Hill, New York, 1980.

2. R.R. Huilgol and N. Phan-Thien, *Fluid Mechanics of Viscoelasticity*, Elsevier, Amsterdam, 1997.

3. C. Ollivier-Gooch and M. Van Altena, A high-order-accurate unstructured mesh finite-volume scheme for the advection-diffusion equation, *Journal of Computational Physics* 181 (2002), 729–752.

4. P.A. Jayantha and I.W. Turner, A second order finite volume technique for simulating transport in anisotropic media, *International Journal of Numerical Methods for Heat & Fluid Flow* 13 (2003), 31–56.

5. E.J. Kansa, H. Power, G.E. Fasshauer and L. Ling, A volumetric integral radial basis function method for time-dependent partial differential equations: I. Formulation, *Engineering Analysis with Boundary Elements* 28 (2004), 1191–1206.

6. T.J. Moroney and I.W. Turner, A finite volume method based on radial basis functions for two-dimensional nonlinear diffusion equations, *Applied Mathematical Modelling* 30 (2006), 1118-1133.

7. T.J. Moroney and I.W. Turner, A three-dimensional finite volume method based on radial basis functions for the accurate computational modelling of nonlinear diffusion equations, *Journal of Computational Physics* 225 (2007), 1409–1426.

8. P. Orsini, H. Power and H. Morvan, Improving volume element methods by meshless radial basis function techniques, *Computer Modeling in Engineering & Sciences* 23 (2008), 187–208.

9. E.J. Kansa, Multiquadrics- A scattered data approximation scheme with applications to computational fluid-dynamics-II. Solutions to parabolic, hyperbolic and el-

liptic partial differential equations, *Computers and Mathematics with Applications* 19 (1990), 147–161.

10. M.S. Ingber, C.S. Chen and J.A. Tanski, A mesh free approach using radial basis functions and parallel domain decomposition for solving three-dimensional diffusion equations, *International Journal for Numerical Methods in Engineering* 60 (2004), 2183-2201.

11. E. Divo and A. Kassab, Iterative domain decomposition meshless method modeling of incompressible viscous flows and conjugate heat transfer, *Engineering Analysis with Boundary Elements* 30(6) (2006), 465–478.

12. B. Sarler and R. Vertnik, Meshfree explicit local radial basis function collocation method for diffusion problems, *Computers & Mathematics with Applications* 51 (2006), 1269–1282.

13. A. Hernandez Rosales, A. La Rocca and H. Power, Radial basis function Hermite collocation approach for the numerical simulation of the effect of precipitation inhibitor on the crystallization process of an over-saturated solution, *Numerical Methods for Partial Differential Equations* 22 (2006), 361–380.

14. G.E. Fasshauer, *Meshfree Approximation Methods With Matlab* (Interdisciplinary Mathematical Sciences - Vol. 6), World Scientific Publishers, Singapore, 2007.

15. N. Mai-Duy and R.I. Tanner, A collocation method based on one-dimensional RBF interpolation scheme for solving PDEs, *International Journal of Numerical Methods for Heat & Fluid Flow* 17 (2007), 165–186.

16. N. Mai-Duy and T. Tran-Cong, A Cartesian-grid collocation method based on radial-basis-function networks for solving PDEs in irregular domains, *Numerical Methods for Partial Differential Equations* 23 (2007), 1192–1210.

17. N. Mai-Duy and T. Tran-Cong, Numerical solution of differential equations using multiquadric radial basis function networks, *Neural Networks* 14 (2001), 185–199.

18. N. Mai-Duy and T. Tran-Cong, Approximation of function and its derivatives using radial basis function networks, *Applied Mathematical Modelling* 27 (2003), 197–220.

19. L. Ling and M.R. Trummer, Adaptive multiquadric collocation for boundary layer problems, *Journal of Computational and Applied Mathematics* 188 (2006), 265–282.

20. C. Shu and Y.L. Wu, Integrated radial basis functions-based differential quadrature method and its performance, *International Journal for Numerical Methods in Fluids* 53 (2007), 969–984.

21. S.A. Sarra, Integrated multiquadric radial basis function approximation methods, *Computers & Mathematics with Applications* 51 (2006), 1283–1296.

22. N.A. Libre, A. Emdadi, E.J. Kansa, M. Rahimian and M. Shekarchi, A stabilized RBF collocation scheme for Neumann type boundary value problems, *Computer Modeling in Engineering & Sciences* 24 (2008), 61–80.

23. H.S. Carslaw and J.C. Jaeger, *Conduction of Heat in Solids*, Clarendon Press, Oxford, 1959.

24. C. Haberland and A. Lahrmann, A comparative investigation on recurrence formulae in finite difference methods, *International Journal for Numerical Methods in Engineering* 25 (1988), 593–609.

25. E. Sanmiguel-Rojas, J. Ortega-Casanova, C. del Pino and R. Fernandez-Feria, A Cartesian grid finite-difference method for 2D incompressible viscous flows in irregular geometries, *Journal of Computational Physics* 204 (2005), 302–318.

26. G. de Vahl Davis, Natural convection of air in a square cavity: a bench mark numerical solution, *International Journal for Numerical Methods in Fluids* 3 (1983), 249–264.

27. P. Le Quere, Accurate solutions to the square thermally driven cavity at high Rayleigh number, *Computers & Fluids* 20 (1991), 29–41.

28. G. Kosec and B. Sarler, Solution of thermo-fluid problems by collocation with local pressure correction, *International Journal of Numerical Methods for Heat & Fluid Flow* 18 (2008), 868–882.

Table 1: Unsteady problem, $0 \leq x \leq 1$, $0 \leq t \leq 0.25$: temperature at the centre of the slab and its percentage error by the present method ($N_x = 5$ and $N_t = 11$) and various finite difference methods (FDMs) ($N_x = 21$ and $N_t = 11$). Results by FDMs (CR: Crank-Nicolson, PI: Pure implicit and WI: Weighted time step) are extracted from [24].

	FDM								
	CN		PI		WT		Present		
t	ϕ	(%)	ϕ	(%)	ϕ	(%)	ϕ	(%)	Analytic
0.025	0.5637	12.35	0.6888	7.09	0.6807	5.84	0.6295	2.12	0.6432
0.05	0.5440	9.69	0.5330	7.47	0.5286	6.58	0.4895	1.28	0.4959
0.075	0.3493	9.68	0.4226	9.27	0.4188	8.29	0.3798	1.80	0.3868
0.1	0.3313	9.66	0.3376	11.76	0.3341	10.58	0.2978	1.41	0.3021
0.125	0.2117	10.31	0.2705	14.58	0.2671	13.14	0.2324	1.54	0.2360
0.15	0.2038	10.50	0.2169	17.60	0.2137	15.86	0.1822	1.22	0.1844
0.175	0.1270	11.84	0.1740	20.74	0.1710	18.67	0.1423	1.26	0.1441
0.2	0.1262	12.10	0.1396	20.99	0.1369	21.57	0.1115	0.93	0.1126
0.225	0.0756	14.12	0.1120	27.33	0.1096	24.54	0.0869	1.17	0.0880
0.25	0.0787	14.47	0.0899	30.76	0.0877	27.58	0.0690	0.37	0.0687

Table 2: Natural convection: Mesh convergence study for the flow of $R_a = 10^7$. "Benchmark*" refer to pseudo-spectral results in [27].

Grid	v_{max}	error(%)	x	u_{max}	error(%)	y	$\overline{N_u}$	error(%)
41×41	620.62	11.24	0.0215	154.80	4.17	0.8763	17.1717	3.93
51×51	668.62	4.37	0.0232	152.29	2.48	0.8765	16.8714	2.11
61×61	692.61	0.94	0.0226	150.93	1.57	0.8770	16.7282	1.24
71×71	700.86	0.24	0.0220	150.24	1.10	0.8775	16.6506	0.77
Benchmark*	699.2		0.021	148.6		0.879	16.523	

Table 3: Natural convection: Comparison between the present solutions using 71×71 and benchmark solutions. "Benchmark" and "Benchmark*" refer to finite-difference and pseudo-spectral results in [26] and [27], respectively.

Method	R_a	v_{max}	error(%)	x	u_{max}	error(%)	y	$\overline{N_u}$	error(%)
Present	10^3	3.6974	0.01	0.1783	3.6494	0.01	0.8132	1.1178	0.02
Benchmark	10^3	3.697		0.178	3.649		0.813	1.118	
Present	10^4	19.6279	0.06	0.1189	16.1834	0.03	0.8232	2.2448	0.08
Benchmark	10^4	19.617		0.119	16.178		0.823	2.243	
Present	10^5	68.632	0.06	0.0659	34.746	0.05	0.8546	4.5219	0.06
Benchmark	10^5	68.59		0.066	34.73		0.855	4.519	
Present	10^6	220.561	0.02	0.0377	64.923	0.14	0.8499	8.8333	0.09
Benchmark	10^6	219.36		0.0379	64.63		0.850	8.880	
Benchmark*	10^6	220.6		0.038	64.83		0.850	8.825	
Present	10^7	700.86	0.24	0.0220	150.24	1.10	0.8775	16.6506	0.77
Benchmark*	10^7	699.2		0.021	148.6		0.879	16.523	

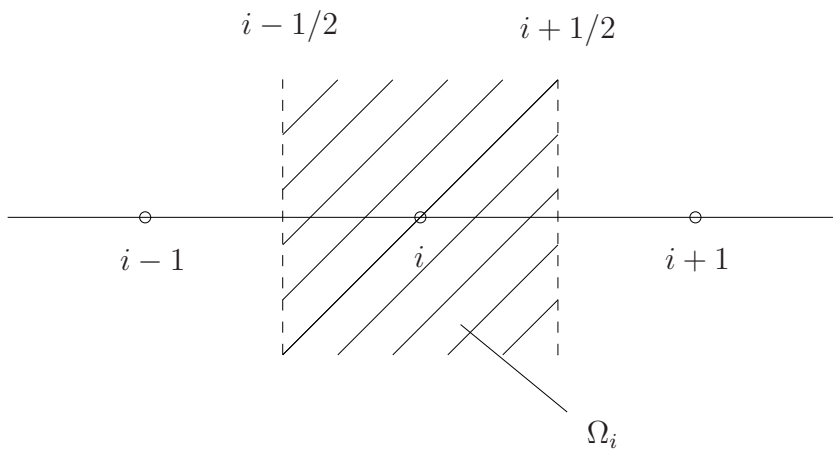

Figure 1: A 1D discretisation scheme: Node i and its associated control volume. The circles represent the nodes, and the vertical dash lines represent the faces of the control volume.

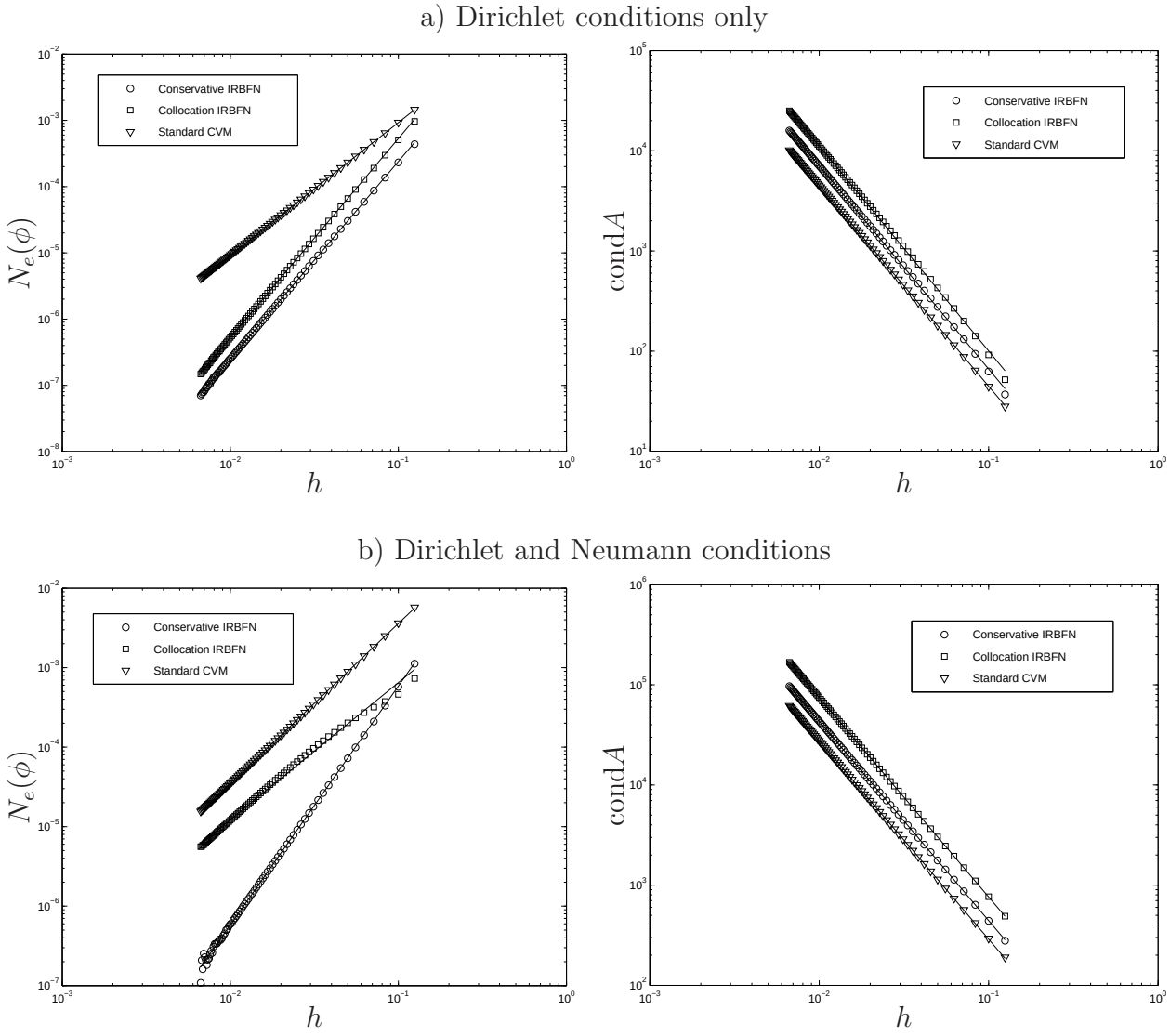

Figure 2: 1D problem, $N_x = [9, 11, 13, \cdots, 151]$: Comparisons of the accuracy and condition number between the conservative IRBFN, collocation IRBFN and standard CV methods. For the case of Dirichlet conditions, their rates respectively are $O(h^{2.98})$, $O(h^{3.00})$ and $O(h^{2.00})$ for the accuracy $N_e(\phi)$, and $O(h^{-2.02})$, $O(h^{-2.04})$ and $O(h^{-2.00})$ for the matrix condition number cond$A$. For the case of Dirichlet and Neumann conditions, they are $O(h^{3.00})$, $O(h^{1.72})$ and $O(h^{2.01})$ for $N_e(\phi)$, and $O(h^{-1.98})$, $O(h^{-1.99})$ and $O(h^{-1.97})$ for cond$A$.

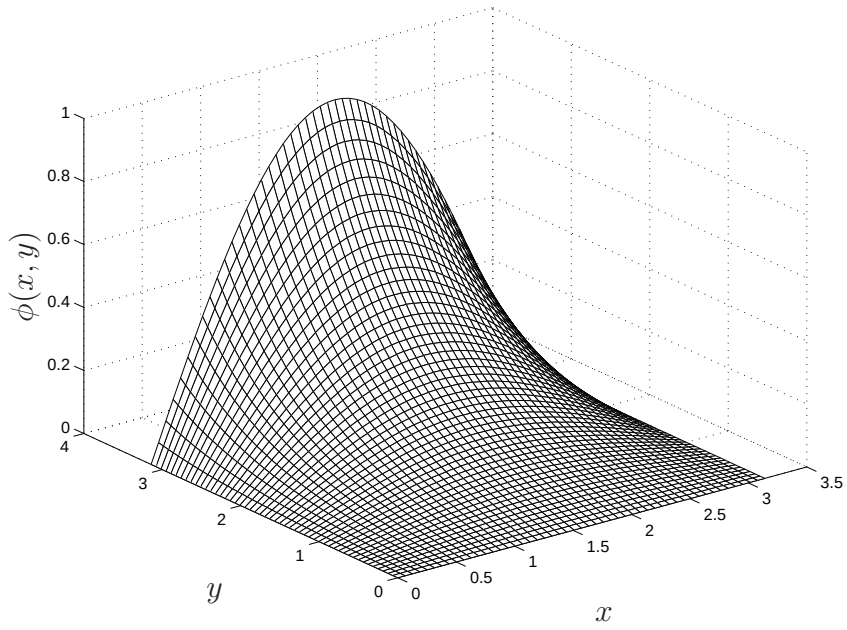

Figure 3: 2D problem: Exact solution.

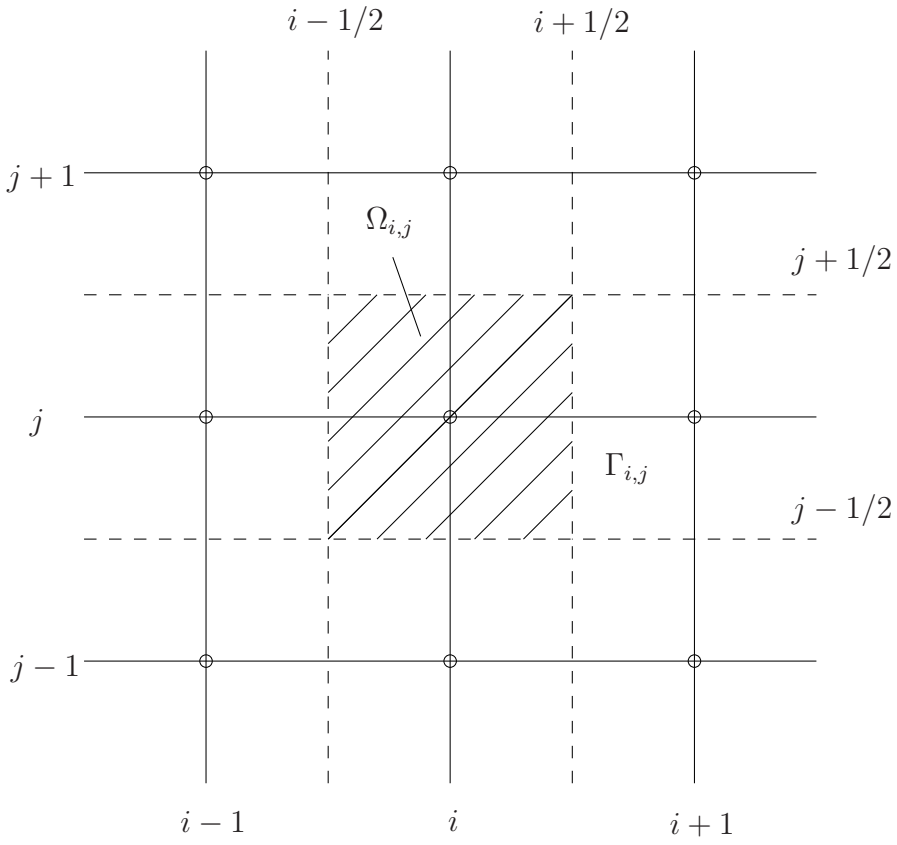

Figure 4: A 2D discretisation scheme: Node (i, j) and its associated control volume $\Omega_{i,j}$. Note that the dash lines represent the faces of the control volume.

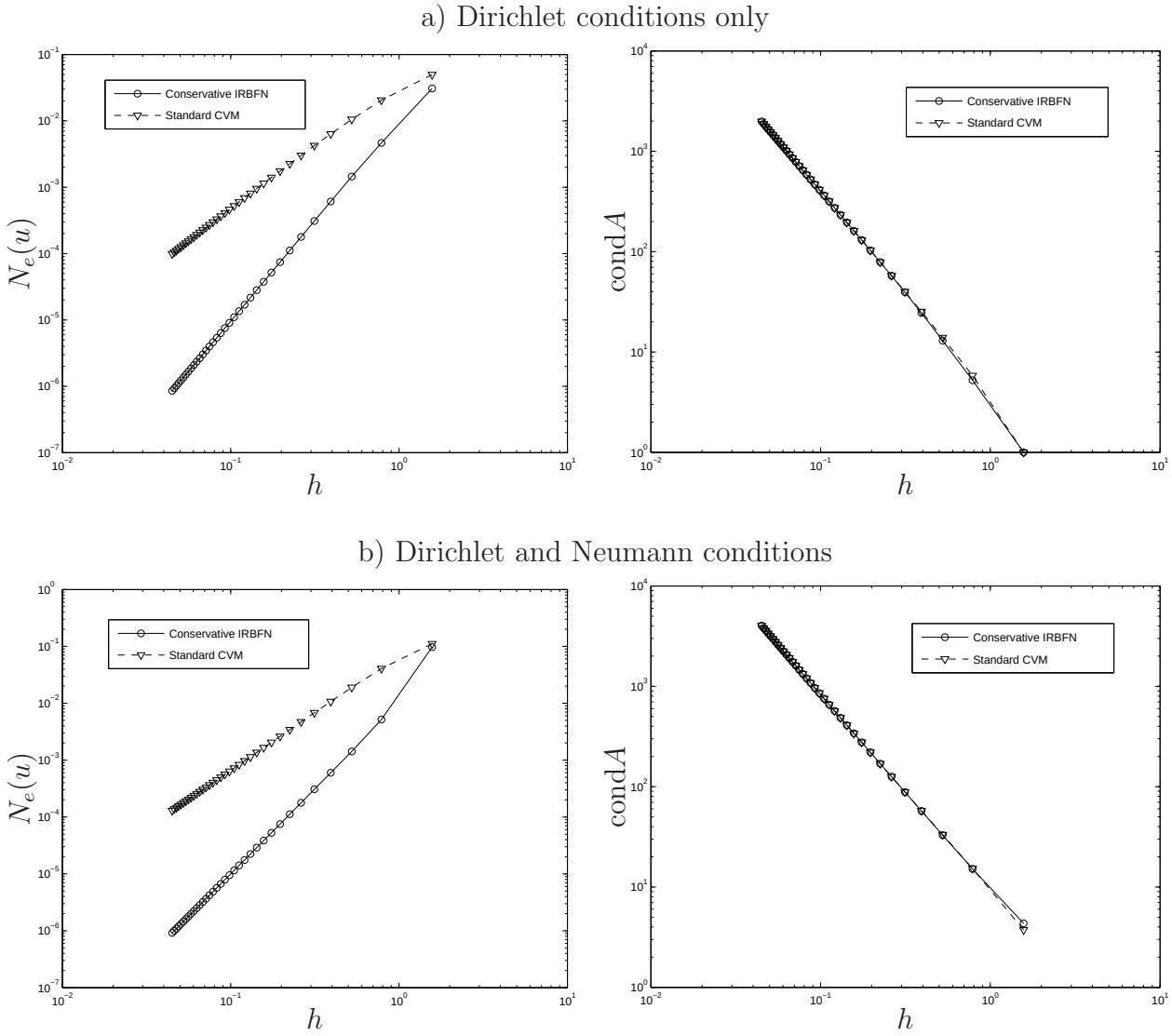

Figure 5: 2D problem, $N = [9, 25, \cdots, 5041]$: Comparisons of the accuracy and condition number between the conservative IRBFN and standard CV methods. For the case of Dirichlet conditions, their rates respectively are $O(h^{3.00})$ and $O(h^{1.84})$ for the accuracy $N_e(u)$, and $O(h^{-2.08})$ and $O(h^{-2.06})$ for the matrix condition number cond$A$. For the case of Dirichlet and Neumann conditions, they are $O(h^{3.09})$ and $O(h^{1.98})$ for $N_e(u)$, and $O(h^{-1.94})$ and $O(h^{-1.96})$ for cond$A$.

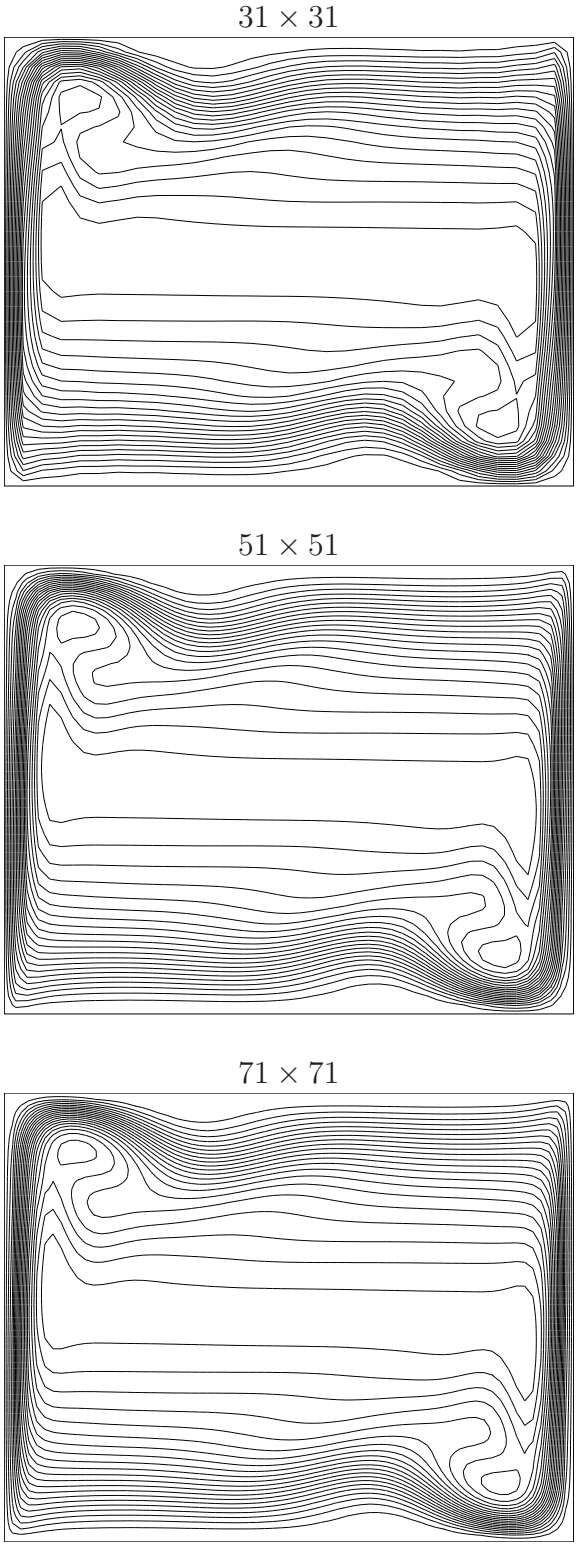

Figure 6: Natural convection, $R_a = 10^7$: Mesh convergence for stream function. Each plot contains 21 contour lines whose values vary linearly. For all grids used, the stream function field seems feasible when compared with the benchmark spectral solution [26].

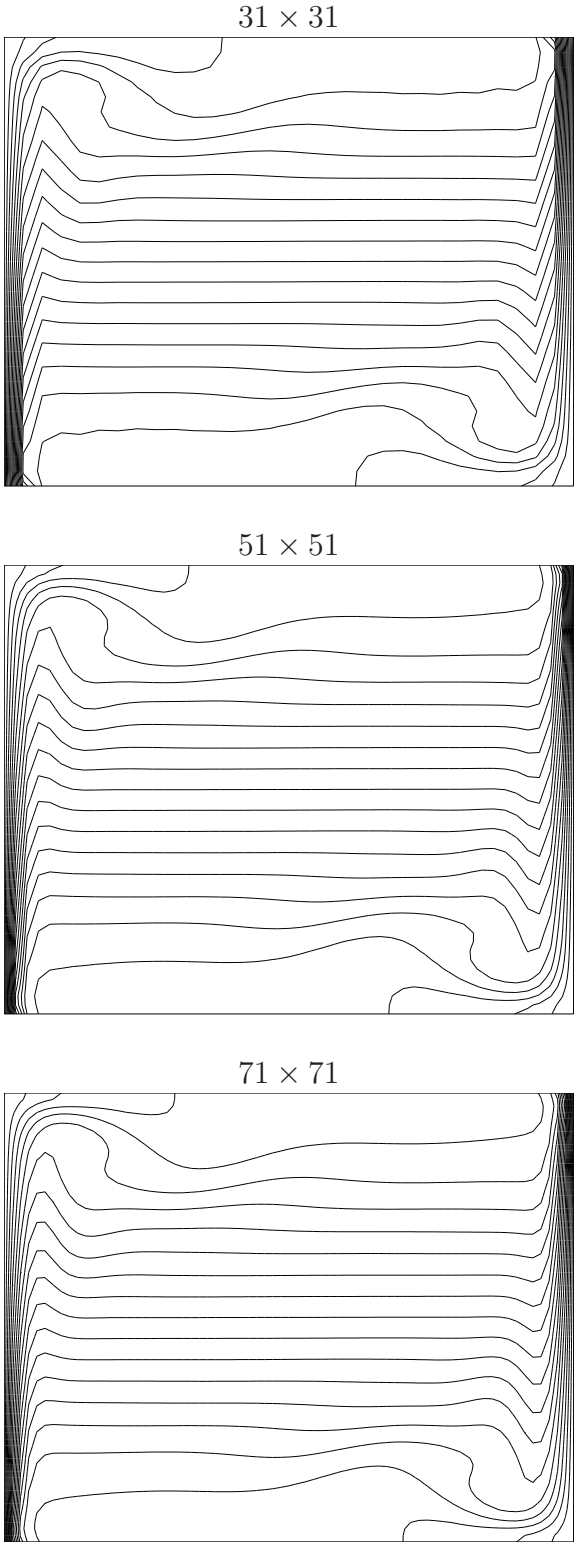

Figure 7: Natural convection, $R_a = 10^7$: Mesh convergence for temperature. Each plot contains 21 contour lines whose values vary linearly. For all grids used, the temperature field looks feasible when compared with the benchmark spectral solution [26].

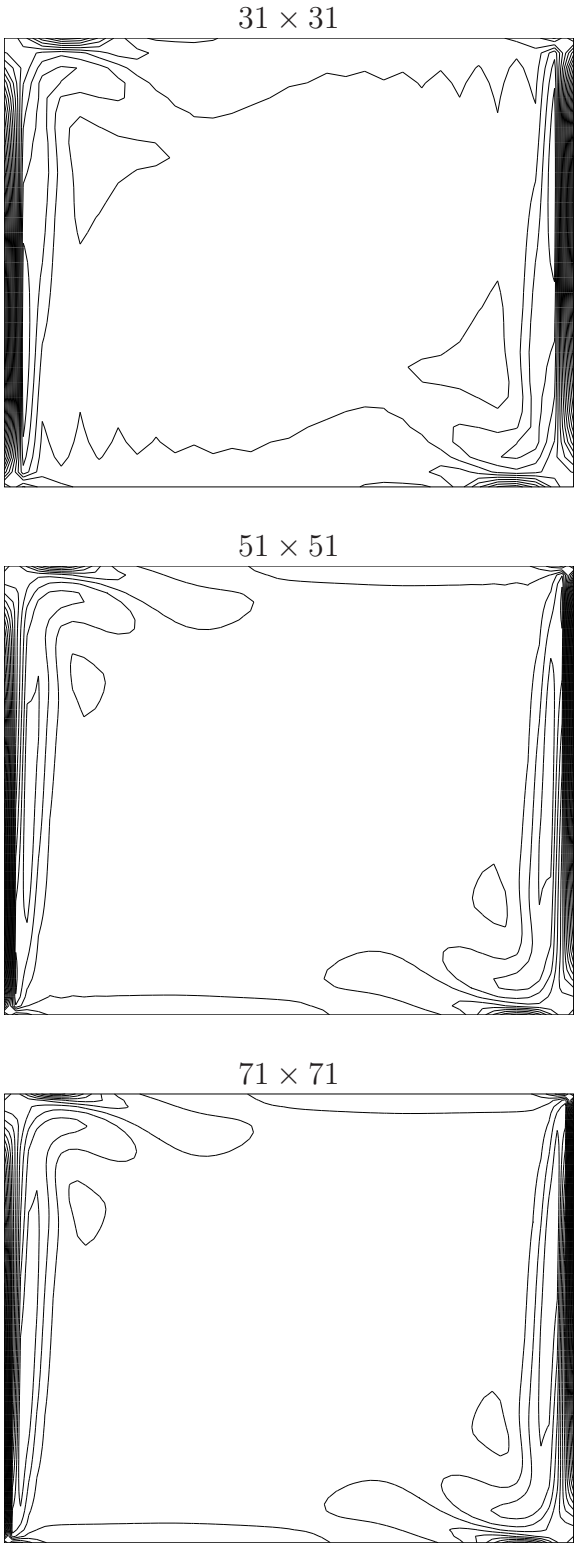

Figure 8: Natural convection, $R_a = 10^7$: Mesh convergence for vorticity. Each plot contains 21 contour lines whose values vary linearly. Unlike stream function and temperature, the vorticity field only becomes feasible when a grid density is 51×51 or greater.